Atomic Force Microscopy (AFM) Study of Poly(ethylene terephthalate-*co*-4,4′-bibenzoate): A Polymer of Intermediate Structure

D. A. SCHIRALDI,[1] M. L. OCCELLI,[2] S. A. C. GOULD[3]

[1] KoSa, P.O. Box 5750, Spartanburg, South Carolina 29304

[2] MLO Consultants, 6105 Blackwater Tr., Atlanta, Georgia 30328

[3] W.M. Keck Science Center, The Claremont Colleges, Claremont, California 91711

Received 28 July 2000; accepted 20 September 2000

ABSTRACT: An atomic force microscope (AFM) operating in both tapping and contact modes was used to study the surface topography and the molecular organization of a molded flexural test bar prepared from a poly(ethylene terephthalate-*co*-4,4'-bibenzoate) copolymer containing a terephthalate:4,4′-bibenzoate molar ratio of 45:55 (PETBB-55). Micrometer-scale (15×15 μm) contact-mode AFM images revealed that the PETBB surface contains a deep indentation that forms trenches that extend over the entire surface examined. In addition, the surface may appear as an overlay of fibrils having different orientation. At greater magnification (1×1 μm), it is possible to observe the existence of micropores. These results were also observed in images obtained while operating the AFM in the tapping mode. The side of the part is more homogeneous and ordered than is its top surface. It has the appearance of a stacked lamellar structure in which missing fibrils can originate cracks ~0.5-μm wide. Fine surface details were observed in nanometer-scale images, showing the presence of chains of white spots that could represent molecules or a cluster of molecules. These chains can form domains in which they are almost parallel to each other and have a preferred orientation; this structural organization was generated without any orientation other than that produced during a mold flow. Alternatively, chain lengths are interrupted and white spots form, distorted by easily recognizable hexagonal arrangements. The degree of lamellar order observed in the side of the bar, the area of greatest flow orientation in the part, was not been observed for the PET homopolymer in the past and bears some resemblance to previously imaged liquid crystalline polyester (LCP) structures. Combined with some previously reported LCP-like mechanical properties, we propose that this PETBB copolymer is, in fact, a "frustrated LCP," one that with some driving force could be converted to liquid crystallinity. © 2001 John Wiley & Sons, Inc. J Appl Polym Sci 82: 2616–2623, 2001

Key words: atomic force microscopy (AFM); injection molding; liquid-crystalline polymers; polyesters; structure

INTRODUCTION

Polyesters produced from the rigid-rod monomer, 4,4′-bibenzoic acid, and many diols (ranging from 1,3-propanediol to 1,12-dodecanediol,[1–5] as well as with triethylene glycol[6,7]) were shown previously to exhibit highly ordered smectic liquid crystalline structures. Copolyether–ester elastomers, produced using the bibenzoate monomer, were also described in the literature[8,9] and can be used to increase operational temperature ranges beyond those of the traditional systems, which

Correspondence to: D. A. Schiraldi.

Journal of Applied Polymer Science, Vol. 82, 2616–2623 (2001)

are based on poly(butylene terephthalate) (PBT). A variety of copolyesters and copolyesteramides[10] that incorporate 4,4′-bibenzoic acid with other dicarboxylic acids (including terephthalic acid,[11] 2,6-naphthalene dicarboxylic acid,[12] 3,4′-bibenzoic acid,[13] and *p*-hydroxybenzoic acid[14]) and one or more diols[4,15,16] were described previously. Some of these rigid-rod copolyesters exhibit liquid crystallinity, while others merely exhibit the properties of rigid, semicrystalline plastics. No clear-cut rule has been postulated for predicting which bibenzoate chemical structures will lead to which type of structure. General interest in commercial applications of bibenzoate-based polyesters may be heightened by a recent report of an efficient, low-cost process for the production of this monomer from toluene.[17]

Among the many polymer systems based on 4,4′-bibenzoate, its copolyesters with terephthalate and ethylene glycol, poly(ethylene terephthalate-*co*-4,4′-bibenzoate) (PETBB) poses an interesting structural challenge.[18,19] The PETBB copolymers can be used to produce rapidly crystallizing, high T_m/T_g, high-modulus semicrystalline polymers suitable for injection molding and other processing methods. PETBB compositions containing greater than 50 mol % bibenzoate can show anisotropic melts and fibrillar damage zones upon breaking, but are not generally liquid crystalline materials.[19,20] Given that the higher homologs of poly(ethylene-4,4′-bibenzoate) are liquid crystalline and that PETBB compositions exhibit many liquid crystalline polyester (LCP)-like characteristics (described by one author as "birefringent" but not liquid crystalline[20]), it is possible that PETBB may exist in an intermediate state of order, in between liquid crystals and semicrystalline solids (a "frustrated LCP"). Despite the previously reported thermomechanical properties of these systems, virtually no structural data for bibenzoate polyesters have been reported to date. It was the purpose of this article to investigate the surface topography of a PETBB molded part using an atomic force microscope (AFM) operating in both contact and tapping modes, to either support or refute the concept of "frustrated liquid crystallinity" in these materials.

EXPERIMENTAL

Polymer/Part Preparation

The preparation of PETBB was described in detail elsewhere.[19] Dimethyl terephthalate, dimethyl-4,4′-bibenzoate (45:55 mol ratio of terephthalate: 4,4′-bibenzoate), and ethylene glycol (2.25 mol glycol:total ester monomers) were condensed in a two-step, 200-kg scale process which utilized manganese acetate and antimony oxide catalysts and poly(phosphoric acid) as a catalyst sequestering agent. When the desired melt viscosity was reached in the polymerization reactor, the polymer was extruded and found to have a measured I.V. of 0.62 on the PET scale (measured as a 4% solution in *o*-chlorophenol). Solid-state polymerization under a vacuum at 210°C for approximately 12 h generated the final polymer, which measured 0.86 I.V. on the PET scale.

Dried PETBB pellets were then injection-molded on a Boy-22S machine equipped with a "family" mold containing an ASTM flexural test bar and a small (5 in.) ASTM tensile bar as parallel branches of the mold. A flat temperature profile of 285°C along the molding machine barrel was used for parts molding, with a 25-s total molding cycle time. The mold temperature was maintained at approximately 45°C using an internally circulating coolant. The molding performance of the PETBB polymer in a mold designed specifically for PBT closely mirrored that of PBT.

AFM Imaging

Sections of an injected-molded PETBB-55 ASTM flexural test bar was glued onto steel disks with epoxy resin. After the glue dried, the AFM tip was carefully guided to the middle of the part to begin the imaging session. The AFM used in this work was a Nanoscope III instrument (from Digital Instruments, Santa Barbara, CA) operating in the contact or tapping mode. The AFM was calibrated using mica. The images presented in this article contain either 256×256 or 512×512 data points and were obtained within a few seconds. The Si_3N_4 cantilevers (with an integral tip) had a length in the 60–120-μm range with a spring constant in the 0.1–0.6-N/m range. The typical force applied to obtain these images ranged from 1.0 to 100 nN. Several hundred images were examined using different cantilevers. To avoid tip-related artifacts, imaging was performed with minimal (less then 10 nN) force and image features were reproduced in both the tapping and contact modes before being accepted as representative.

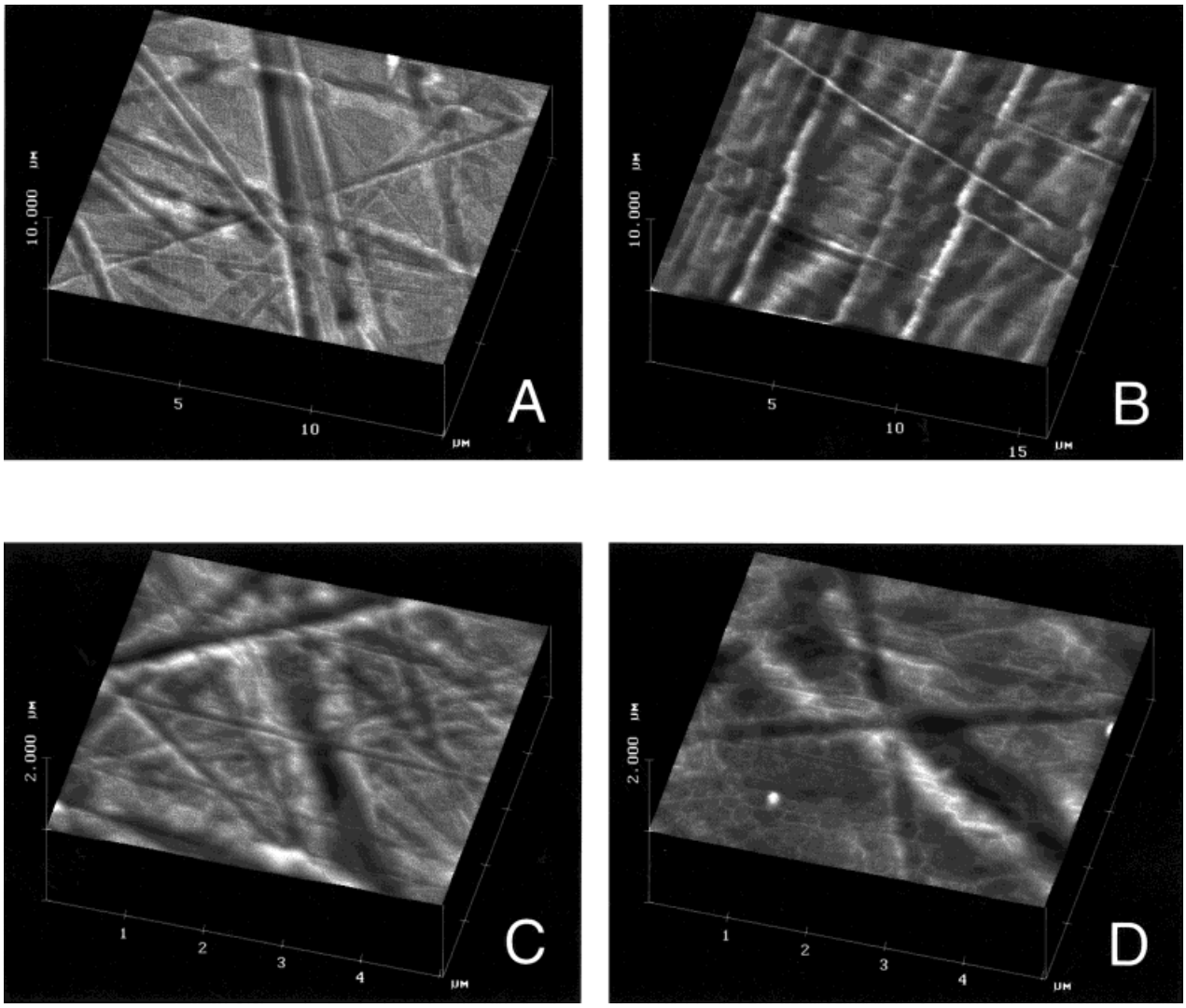

Figure 1 Contact-mode AFM images of the PETBB surface showing (A) surface indentations, (B) surface fibrils, and (C) the existence of raised surface features. (D) Reproduction of surface details while operating the AFM in the tapping mode.

RESULTS AND DISCUSSION

Since its invention in 1986, AFM has evolved into an imaging technique of solid surfaces that is capable of providing resolution not accessible by other microscopic techniques, such as SEM.[21,22] AFM has been particularly useful to study the surface architecture and molecular chain structure of many polymers, including semicrystalline PET.[23–25] In our previous work, AFM images were used to describe the surface of PET[23,24] and of liquid crystalline poly(hydroxybenzoate–hydroxynaphthoate) polymers films[25] with nanometer-scale resolution. It was shown that imaging forces can alter the PET film surface[24,26]; surface deformation can be minimized by operating the AFM in a tapping mode. It is for these reasons that, in the present study, law force imaging was performed with a weak cantilever having a force constant of 0.6 N/m.

The choice of a PETBB copolymer sample containing 55 mol % 4,4′-bibenzoate was made for this study because previous work showed this specific composition to match the T_m of PET (but with the T_g enhanced by 20°C) to be readily produced in commercial PET manufacturing equipment. Moreover, in contrast to the properties of the PET homopolymer, this composition exhibits anisotropic melts and fibrillar (splintered wood-like) damage zones when broken, reminiscent of LCPs.[19] Combined with the relative ease with which it can be injection-molded, PETBB-55

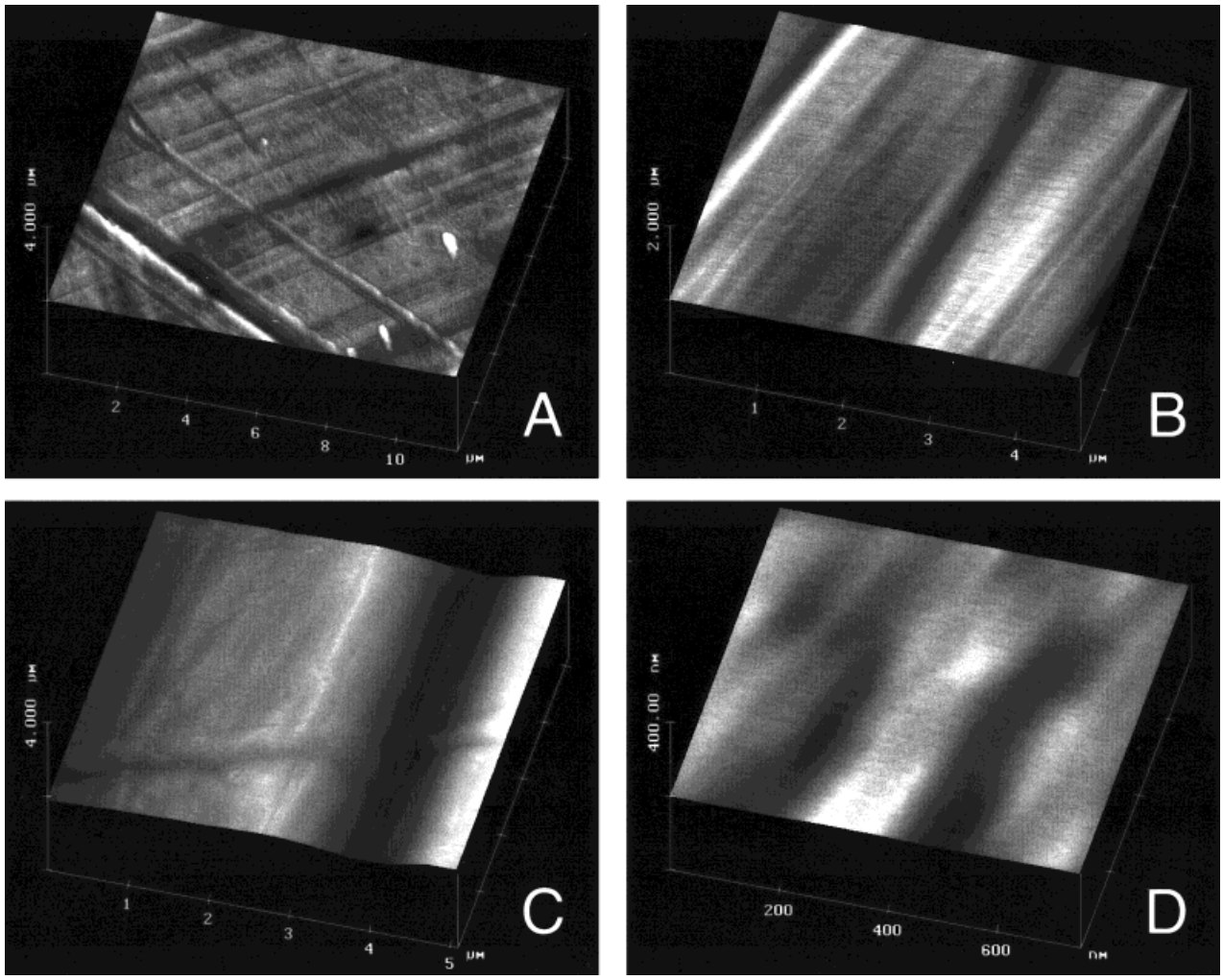

Figure 2 Contact-mode AFM images of the PETBB film side showing (A) the stacked lamellar structure, (B) details of the stacked lamellar structure, (C) missing fibrils and the generation of a large void in the stack, and (D) the decomposition of a large fibrils into three smaller ones.

shows promise as a higher-temperature alternative to both PBT and PET in molding applications.

Micrometer-scale AFM images of the PETBB sample are shown in Figures 1 and 2. The surface of the molded bar appears fairly inhomogeneous and contains deep indentations that generate trenches extending over the entire surface. In Figure 1(A), the various indentations do not have a preferred orientation and can be 1.4 μm wide and 40 nm deep. These cracks could be the results of longitudinal and lateral forces that exist during the molding process or could result from surface scratches in the injection mold. The PETBB surface seems to support fibrils 0.5 μm wide and 25 nm in height [Fig. 1(A)]. The existence of regions covered by surface fibrils having different orientation can be seen in Figure 1(B). The left-hand side of this figure resembles the images obtained for PET films.[22] In this figure, it is possible to observe a bundle of fibrils (separated by an average distance of 0.7 μm) followed by an amorphous region about 4.3 μm wide. The right side of the image is less ordered; fibrils cover the film surface without displaying a preferred orientation. The lack of fibrillar orientation together with the presence of indentations as seen in Figure 1(A–C) are fairly common features of the surface of the bar. In Figure 1(C), the indentation on the surface is 370 nm wide and 20 nm deep. Similar surface details were also observed when operating the AFM in a tapping mode; compare Figure 1(A) with Figure 1(D).

The PETBB molded bar under study is approximately 5 mm thick, thus allowing imaging of its

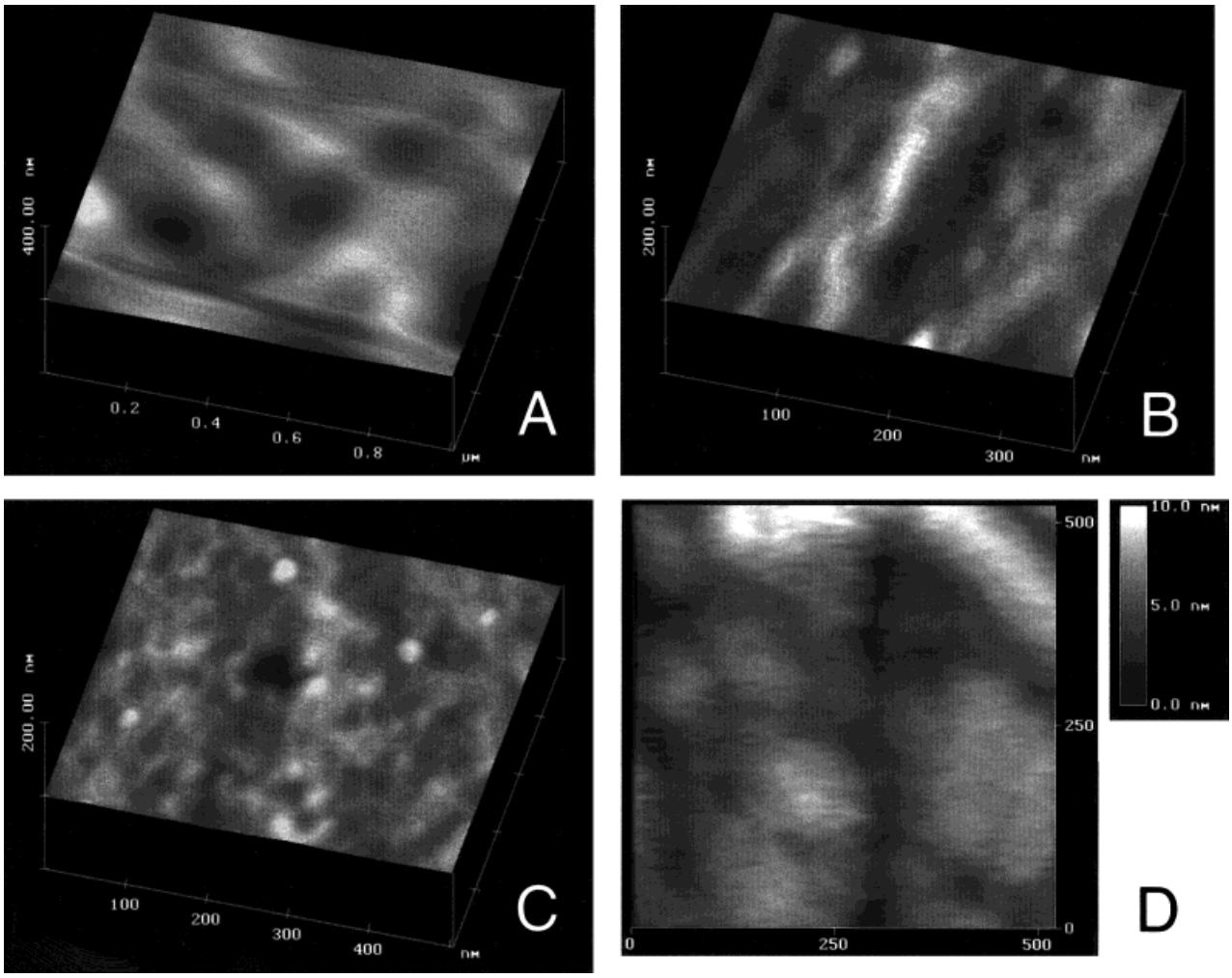

Figure 3 Contact-mode AFM images of the PETBB surface showing (A) the existence of surface nanopores, (B) surface porosity from images obtained while operating the AFM in the tapping mode, (C) tapping-mode AFM image showing the presence of granules and the formation of chains, and (D) voids between chains.

side. The micrometer-scale image of the part side in Figure 2(A) contains many of the features observed on its top surface; see Figure 1(A). The surface of the part's side does appear more homogeneous and ordered than does the top surface [Fig. 2(B)]. In fact, the side has a layered appearance and seems composed of fibrils arranged in stacks of variable thickness. In Figure 2(A), the thickness of the stacks is in the 2.0–3.5-μm range and the average width of a fibril is about 400 nm; a stack of fibrils can be separated by a trench 0.4 μm wide as in Figure 2(A). In Figure 2(B), it is possible to observe two stacks having a width of 2.5 and 1.6 μm, respectively, separated by a trench 0.3 μm wide. Fibrils with a diameter in the 120–180-nm range can be observed in these stacks. Sometimes, the stacked lamellar structure is overlaid by fibrils or crossed by channels as in Figure 2(A). The layered structure of the side may be interrupted by deep cracks that can be 2.8 μm wide and 200 nm deep [see Fig. 2(C)]. At a greater magnification, the side of the part appears composed of the stacking of fibrils about 0.2 μm wide that can coalesce into a single fibril as shown in Figure 2(D).

At greater magnification, as in the 1 $\times$ 1-μm image in Figure 3(A), it is possible to observe that the part surface can contain pores with widths in the 175–200-nm range and 5 nm deep. This surface porosity can be observed also in the tapping-mode AFM image in Figure 3(B). Surface details begin to appear in the nanometer-scale images in Figure 3(C,D). Granules, irregular in size and shape, may protrude above the part surface or

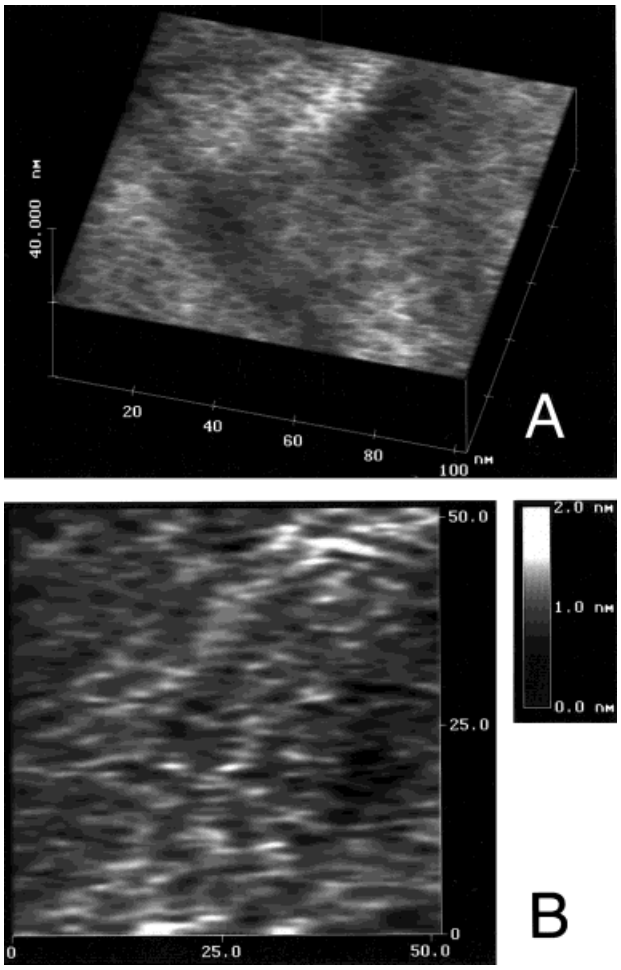

Figure 4 Nanometer-scale contact-mode AFM images of the PETBB surface: (A) structural details of a 100 × 100-nm surface; (B) the surface at a greater magnification.

may coalesce to form raised ridges as in Figure 3(C) or larger particles as in Figure 3(D). Surface structures begin to be observable in Figure 4. Small white spots connect to form a lacelike structure that covers the domain investigated [Fig. 4(A)]. The fine surface details in Figure 4(B) represent the surface as an agglomeration of chains of molecules aligned along what appears to be a preferred orientation.

The existence of well-ordered domains can be seen in the 10 × 10-nm image in Figure 5(A). It is proposed that the white spots represent molecules or a cluster of molecules, arranged in almost a parallel alignment. Disordered domains as in Figure 5(B) are a fairly common occurrence. A distorted, but easily recognizable hexagonal arrangement of six white spots can be seen in this figure. Additional structural details of the surface can be observed in the molecular-scale images in Figure 5(C,D). Cross-sectional analysis of the surface in Figure 5(C) indicates that the row of white spots are 0.20 nm apart and that the individual white spots are about 0.25 nm wide and ~0.10 nm in height. Possible branch points are visible in this figure. When this occurs, the surface becomes less ordered and rows (or chains) of white spots are no longer easily identifiable [see Fig. 5(D)]. Although rows are no longer present, hexagons of white spots are, nonetheless, present in this figure and in other images now included in this article.

SUMMARY AND CONCLUSIONS

Micrometer-scale (15 ×15 μm) contact-mode AFM images revealed that the PETBB-55 surface contains a deep indentation that forms trenches that extend over the entire surface examined. In addition, the surface may appear as an overlay of fibrils having different orientation. At greater magnification (1 × 1 μm), it is possible to observe the existence of micropores. These results were also observed in images obtained while operating the AFM in a tapping mode. The side of the molded bar is more homogeneous and ordered than is its top surface. It has the appearance of a stacked lamellar structure in which missing fibrils can originate cracks ~0.5 μm wide. Fine surface details were observed in nanometer-scale images showing the presence of chains of white spots that could represent molecules or a cluster of molecules. These chains can form domains in which they are almost parallel to each other and have a preferred orientation; this structural organization was generated without any orientation other than that generated during the mold flow. Alternatively, the chain lengths are interrupted and white spots form, distorted by easily recognizable hexagonal arrangements. The degree of lamellar order observed in the side of the part, and area of greatest flow orientation in the part, was not observed for the PET homopolymer in the past and bears some resemblance to previously imaged LCP structures.

These results, and previously reported LCP-like melts and fracture properties, appear to indicate that the PETBB copolymer is, in fact, a "frustrated LCP," one that with some driving force could be converted to liquid crystallinity. Development of a means of transforming the PETBB-55 into a liquid crystalline state, combined with new routes to low-cost bibenzoate

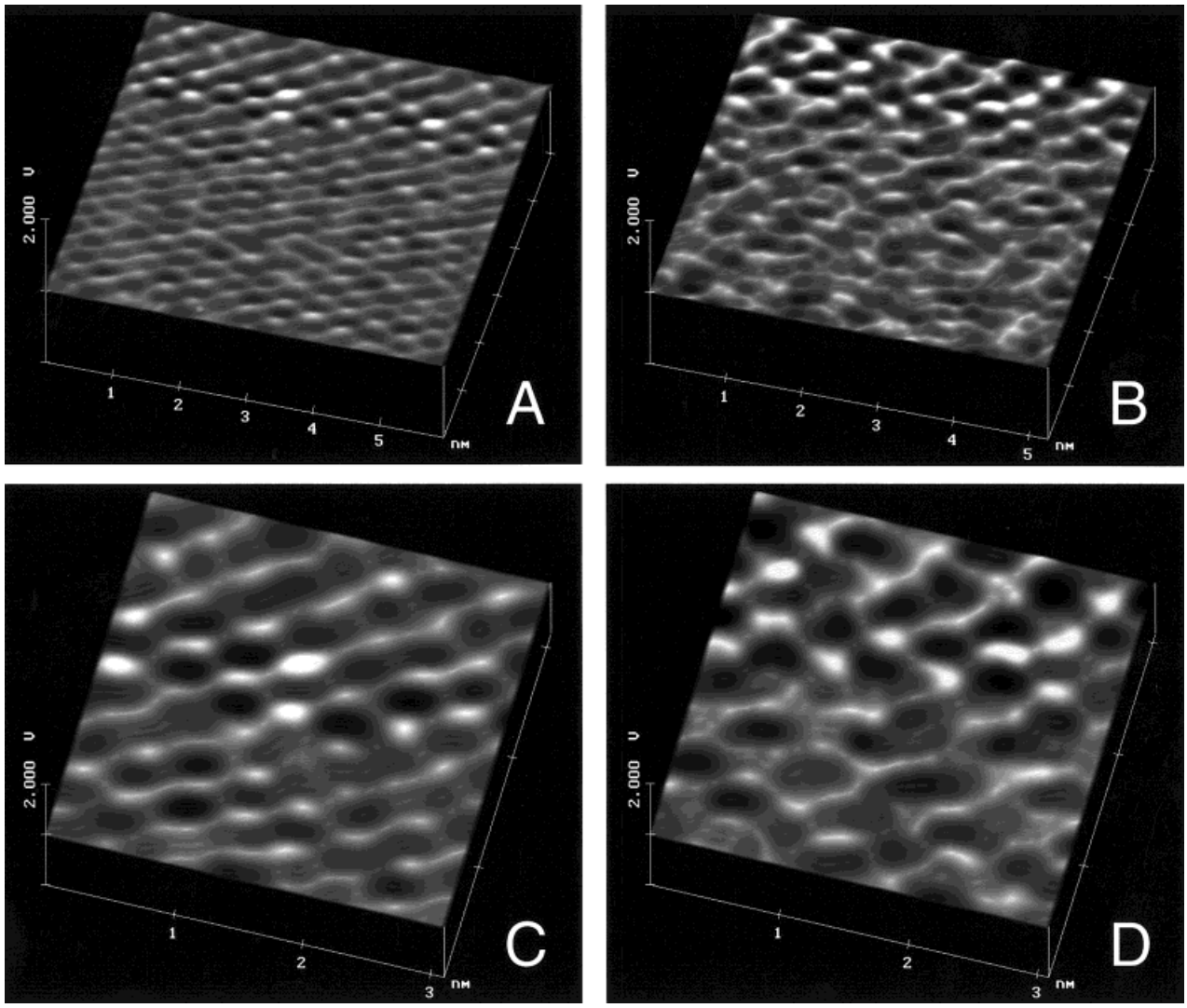

Figure 5 Molecular-scale contact-mode AFM images of the PETBB surface, after application of a 2D FFT routine with the FFT attenuation band cutoff set to 8: (A) well-oriented chains; (B) less ordered domain, with hexagonal arrangement of white spots evident; (C) details of an ordered domain; (D) a disordered domain containing hexagonal rings.

monomers and the relative ease of producing bibenzoate copolymers, could bring about changes in the types of high-performance structural polymers available in the marketplace.

REFERENCES

1. Lee, D.-K.; Tsai, H.-B. J Appl Polym Sci 1997, 65, 893–900.
2. Jackson, W. J.; Morris, J. C. ACS Symposium Series 435 (Liquid Crystal Polymers); American Chemical Society: Washington, DC, 1990; pp 16–32.
3. Jackson, W. J.; Morris, J. C. U.S. Patent 5 037 946 (to Eastman Kodak Co.), 1991.
4. Jackson, W. J.; Morris, J. C. U.S. Patent 5 011 878 (to Eastman Kodak Co.), 1991.
5. Jackson, W. J.; Morris, J. C. U.S. Patent 4 959 450 (to Eastman Kodak Co.), 1990.
6. Perez, E.; Zhu, Z.; Bello, A.; Perena, J. M.; Benavente, R. Eur Polym J 1996, 32, 631–634.
7. Perez, E.; Benevente, R.; Bello, A.; Perena, J. M.; VanderHart, D. L. Macromolecules 1995, 28, 6211–6218.
8. Lee, H.-B.; Liu, D.-K.; Tsao, Y.-S.; Tsai, R.-S. J Appl Polym Sci 1996, 59, 1027–1031.
9. Tsai, H.-B.; Lee, D.-K.; Liu, J.-L.; You, J.-W. J Polym Res 1995, 2, 109–114.

10. Gupta, B.; Halke, W.; Shepherd, J. P.; Sawyer, L. C. World Patent 95/17 446 (to Hoechst Celanese Corp.), 1995.
11. Krigbaum, W. R.; Asrar, J.; Torkiumi, H.; Ciferri, A.; Preston, J. J Polym Sci Polym Lett 1982, 20, 109–115.
12. Choe, E. W;. Flint, J. A. U.S. Patent 5 453 321 (to Hoechst Celanese Corp.).
13. Mang, M. N.; Brewbaker, J. L. U.S. Patent 5 138 022 (to Dow Chemical Co.), 1992.
14. Alms, G. R.; Samual, M. R.; Waggoner, M. G. U.S. Patent 5 250 654 (to E.I. DuPont de Nemours and Co.), 1993.
15. Morris, J. C.; Jackson, W. R., Jr. U.S. Patent 5 057 595 (to Eastman Kodak Co.), 1991.
16. Morris, J. C.; Jackson, W. R., Jr. U.S. Patent 5 037 947, 1991.
17. Sherman, S. C.; Iretskii, A. V.; White, M. G.; Schiraldi, D. A. Chem Innov 2000, 30(7), 25–30.
18. Asrar, J.; Berger, P. A.; Weinkauff, D. J. J Appl Polym Sci 1996, 59, 1001–1008.
19. Brown, D. M.; Clary, R. S.; Lee, C. D.; Monroe IV, W. G.; Vaughn, D. A.; Ragheb, R. T.; Erter III, J. W.; Schiraldi, D. A. Polym Prepr 2000, 41, 123.
20. Krigbaum, W. R.; Asrar, J.; Toriumi, H.; Ciferri, A.; Preston, J. J Polym Sci Polym Lett Ed 1982, 20, 109–115.
21. Binnig, J.; Rohrer, H.; Gerber, C.; Weibel, E. Phys Rev Lett 1983, 50,120.
22. Albrecht, T. R.; Dovek, M. M.; Lang, C. A.; Grutter, P.; Quate, C. F.; Kuan, S. N. J.; Frank, C. W.; Pease, R. F. W. J Appl Phys 1988, 64, 1178.
23. Gould, S. A. C.; Occelli, M. L.; Schiraldi, D. A. J Appl Polym Sci 1997, 65, 1237–1243.
24. Occelli, M. L.; Schiraldi, D. A.; Gould, S. A. C. CHEMTECH 1998, 28, 35–39.
25. Hays, N. W.; Beamson, G.; Clark, D. T.; Law, D. S.-L. Polymer 1996, 37, 523–526.
26. Gould, S. A. C.; Shulman, J. B.; Schiraldi, D. A.; Occelli, M. L. J Appl Polym Sci 1999, 74, 2243–2254.